JOURNAL OF GEOPHYSICAL RESEARCH, VOL. 113, C07052, doi:10.1029/2007JC004328, 2008

Complexity of the flooding/drying process in an estuarine tidal-creek salt-marsh system: An application of FVCOM

Changsheng Chen,[1,5] Jianhua Qi,[1] Chunyan Li,[2,5] Robert C. Beardsley,[3] Huichan Lin,[4] Randy Walker,[4] and Keith Gates[4]

Received 9 May 2007; revised 15 March 2008; accepted 7 April 2008; published 30 July 2008.

[1] The tidal flooding/drying process in the Satilla River Estuary was examined using an unstructured-grid finite-volume coastal ocean model (FVCOM). Driven by tidal forcing at the open boundary and river discharge at the upstream end, FVCOM produced realistic tidal flushing in this estuarine tidal-creek intertidal salt-marsh complex, amplitudes and phases of the tidal wave, and salinity observed at mooring sites and along hydrographic transects. The model-predicted residual flow field is characterized by multiscale eddies in the main channel, which are verified by ship-towed ADCP measurements. To examine the impact of complex coastal geometry on water exchange in an estuarine tidal-creek salt-marsh system, FVCOM was compared with our previous structured-grid finite difference Satilla River Estuary model (ECOM-si). The results suggest that by failing to resolve the complex coastal geometry of tidal creeks, barriers and islands, a model can generate unrealistic flow and water exchange and thus predict the wrong dynamics for this estuary. A mass-conservative unstructured-grid model is required to accurately and efficiently simulate tidal flow and flushing in a complex geometrically controlled estuarine dynamical system.

Citation: Chen, C., J. Qi, C. Li, R. C. Beardsley, H. Lin, R. Walker, and K. Gates (2008), Complexity of the flooding/drying process in an estuarine tidal-creek salt-marsh system: An application of FVCOM, *J. Geophys. Res.*, *113*, C07052, doi:10.1029/2007JC004328.

1. Introduction

[2] Many estuaries, lagoons, inlets, and bays are characterized by complex irregular geometries with islands, barriers, tidal creeks, and intertidal salt marshes. The Satilla River Estuary, located on the southern coast of Georgia, has an averaged depth of ~4 m and a width varying from 5 km at the mouth to less than 100 m at the upstream head (Figure 1). It is a typical tidally controlled estuary covered by extensive intertidal salt marshes and numerous tidal creeks, small islands, and barriers. The area of the salt marsh is ~300 km^2, which is about 2.6 times as large as the total area of the main channels, branches and tidal creeks.

[3] Water movement in the Satilla River Estuary is driven mainly by tidal forcing and river discharge. The tides are dominated by the semidiurnal M_2 constituent, with an amplitude of ~1 m or higher in surface elevation and a current of ~0.3–0.5 m/s. During spring tide, the maximum tidal range can exceed 3 m, at which time the water can flush over the entire salt marsh area bounded by a 2-m elevation line. Ignoring the area of the intertidal salt marsh not only causes a 50% underestimate of the amplitude of tidal currents, but also fails to capture tidal flushing dynamics from the shelf into the estuary [*Zheng et al.*, 2003a].

[4] The annual average rate of freshwater discharge into the Satilla River Estuary is less than 100 m^3/s, with a maximum value of 150 m^3/s in late winter. Temporal and spatial variations of salinity are controlled mainly by tidal mixing between the freshwater input from the upstream head and salt water intruding from the inner shelf of the South Atlantic Bight (SAB). A vertical salinity front is observed at the boundary of these two water masses, where it is generally well mixed vertically due to strong tidal mixing.

[5] *Zheng et al.* [2003a] simulated the tidally and freshwater-discharge driven currents as well as tidal flushing over the estuarine intertidal salt-marsh complex in the Satilla River Estuary by implementing a 3D wet/dry point treatment method into the modified Princeton Ocean Model called ECOM-si, a structured-grid finite difference model [*Blumberg*, 1994]. This model was robust and produced the volume of water flushed into/drained out of the estuary and the longitudinal salinity distribution. A key finding from this experiment suggests that the Satilla River Estuary is a geometrically controlled dynamical system in which the

[1] School for Marine Science and Technology, University of Massachusetts-Dartmouth, New Bedford, Massachusetts, USA.
[2] Coastal Studies Institute, Department of Oceanography and Coastal Sciences, School of the Coast and Environment, Louisiana State University, Baton Rouge, Louisiana, USA.
[3] Department of Physical Oceanography, Woods Hole Oceanographic Institution, Woods Hole, Massachusetts, USA.
[4] Marine Extension Service, University of Georgia, Athens, Georgia, USA.
[5] Marine Ecosystem and Environmental Laboratory, Shanghai Ocean University, Shanghai, China.

0148-0227/08/2007JC004328$09.00

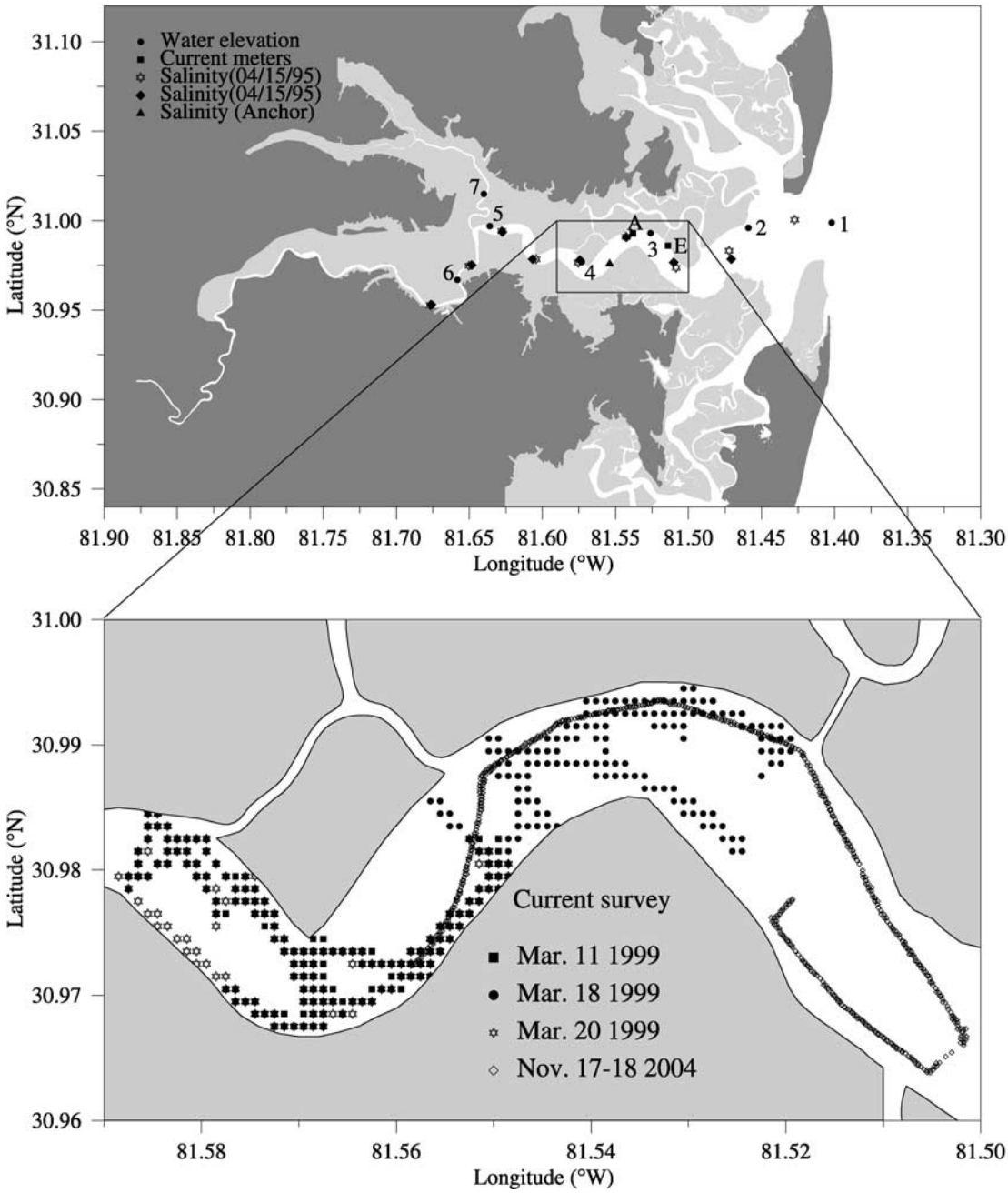

Figure 1. Geometry of the Satilla River Estuary. Light gray filled area: the intertidal salt marsh zone bounded by the 2-m elevation line; (A) and (E): the locations of the two current meter mooring sites, filled circles: the bottom pressure measurement sites numbered 1 to 7; stars: the along-estuary CTD measurement stations; filled triangle: the anchor site for the time series salinity measurements. Solid lines: the ship-towed ADCP tracks.

spatial structure of tidal and residual currents depends strongly on local bathymetry and the curved coastline [*Zheng et al.*, 2003a]. However, this model is limited in resolving the complex geometry of the narrow tidal creeks, upstream branches, islands and barriers, and thus it failed to produce realistic water exchange over the river-tidal creek-intertidal salt marsh complex within this estuary.

[6] An unstructured-grid Finite-Volume Coastal Ocean Model (FVCOM) was then developed to take advantage of the finite element methods in geometrical flexibility and finite difference methods in computational efficiency for estuarine applications [*Chen et al.*, 2003]. The triangular grid used in FVCOM makes this model capable of resolving complex estuarine geometry and bathymetry. A 3D mass-conservative wet/dry treatment implemented in this model allows us to simulate the flooding/drying process in an estuarine system with numerous tidal creeks and extensive intertidal salt marshes. FVCOM was first applied to the Satilla River Estuary and validated through extensive model-data comparisons. Further development of FVCOM has

followed, and it is now being used for global, regional, and coastal ocean as well as estuarine applications (see FVCOM website: http://fvcom.smast.umassd.edu).

[7] This paper examines the impact of complex estuarine geometry on tides, residual currents, and water exchange processes in the Satilla River Estuary through comparisons with measurements of tidal elevation, residual current and salinity. A comparison is also made between FVCOM and ECOM-si to illustrate and emphasize the importance of resolving tidal creeks, islands and barriers for realistic water exchange over the estuarine tidal-creek salt-marsh complex in the Satilla River Estuary.

[8] The paper is organized as follows. In section 2, FVCOM and the numerical experiments are described. In section 3, tidal flooding/drying processes over the estuarine tidal-creek intertidal salt-marsh complex are simulated and the model-data comparisons presented. In section 4, results of the salinity simulation are presented. In section 5, an intermodel comparison between FVCOM and ECOM-si is given. In section 6, conclusions are presented.

2. FVCOM and Experimental Design

[9] FVCOM is an unstructured-grid, finite-volume, 3D primitive equation free-surface coastal ocean model developed originally by *Chen et al.* [2003]. The early version of this model (used in this study) was configured using the σ-transformation in the vertical and a nonoverlapping, unstructured triangular grid in the horizontal. The governing equations were closed with a default setup of the Mellor and Yamada level 2.5 turbulent closure scheme for vertical eddy viscosity [*Mellor and Yamada*, 1982] and the Smagorinsky eddy parameterization for horizontal diffusion coefficients [*Smagorinsky*, 1963], with an alternative selection of the General Ocean Turbulence Model (GOTM) modules [*Burchard*, 2002]. FVCOM has been improved by a team of UMASSD and WHOI researchers [*Chen et al.*, 2004, 2006a, 2006b, 2007; *Cowles*, 2008]. The updated version is cast in a generalized terrain-following coordinate system with spatially variable vertical distribution [*Pieterzak et al.*, 2002]. A detailed description of FVCOM was given in the FVCOM user manual [*Chen et al.*, 2006a] and in an introduction paper [*Chen et al.*, 2006b].

[10] The governing equations of FVCOM are the same as the popular finite difference models such as the Princeton Ocean Model (POM), the semi-implicit version of POM (ECOM-si), and the Regional Ocean Model (ROMs). Similar to POM and ROMs, FVCOM is numerically solved by a mode splitting method. The external mode is composed of vertically integrated transport equations in which the water elevation is solved explicitly using a shorter time step constrained by the ratio of the horizontal resolution to the phase speed of the surface gravity wave. The internal mode consists of the full 3D governing equations and is solved using a longer time step constrained by the phase speed of the lowest mode internal wave. Linkage between external and internal modes is through the water elevation, with mode adjustments at each internal time step. Unlike finite difference and finite element models, the spatial fluxes of momentum are discretized using a second-order accurate unstructured-grid finite-volume method [*Kobayashi et al.*, 1999]. Scalar (e.g., temperature and salinity) equations are solved using a second-order upwind flux scheme and in conjunction with a vertical velocity adjustment to enforce exact conservation of the scalar quantities. The finite-volume method used in FVCOM not only takes the advantage of finite element methods in geometric flexibility and finite difference methods in computational efficiency, but also ensures volume and mass conservation in individual control volumes.

[11] The flooding/drying process in FVCOM is simulated using an unstructured wet/dry point treatment technique [*Chen et al.*, 2006a; C. Chen et al., A wet/dry point treatment method of FVCOM. part I: Stability experiments, submitted to *Ocean Modeling*, 2008]. A viscous sublayer with a thickness $D_{\min}$ is added into the model to avoid the occurrence of singularity when the local water depth approaches zero. In this system, the wet or dry criterion for node points is

$$\begin{cases} \text{wet}, & \text{if } D = H + \zeta + h_B > D_{\min} \\ \text{dry} & \text{if } D = H + \zeta + h_B \le D_{\min} \end{cases} \tag{1}$$

and for triangular cells is

$$\begin{cases} \text{wet}, & \text{if } D = \min\left(h_{B,\hat{i}}, h_{B,\hat{j}}, h_{B,\hat{k}}\right) + \max\left(\zeta_{\hat{i}}, \zeta_{\hat{j}}, \zeta_{\hat{k}}\right) > D_{\min} \\ \text{dry}, & \text{if } D = \min\left(h_{B,\hat{i}}, h_{B,\hat{j}}, h_{B,\hat{k}}\right) + \max\left(\zeta_{\hat{i}}, \zeta_{\hat{j}}, \zeta_{\hat{k}}\right) \le D_{\min} \end{cases} \tag{2}$$

where h_B is the bathymetric height related to the edge of the main channel of an estuary; $\hat{i}$, $\hat{j}$ and $\hat{k}$ are integer numbers to identify the three node points of a triangular cell; H is the mean water depth; and ζ is the surface elevation. When a triangular cell is treated as dry, the velocity at the centroid of this triangle is specified to be zero and no flux is allowed through the three side boundaries of this triangle. This triangular cell is removed from the flux calculation in the tracer control elements. In this study, $D_{\min}$ = 5.0 cm. The wet/dry treatment code was validated for both idealized and realistic estuarine cases, and a detailed discussion was given by Chen et al. (submitted manuscript, 2008).

[12] The computational domain covered the entire Satilla River Estuary including the main channels, tidal creeks and intertidal salt-marshes (Figure 2). The model was discretized using nonoverlapping triangular cells with a horizontal resolution of 40 to 100 m in the main channels and over intertidal salt marshes, and up to 2500 m close to the open boundary on the inner shelf. Eleven sigma-levels were used in the vertical, which allows for smooth representation of finite-amplitude irregular bottom bathymetry. These levels corresponded to a vertical resolution of 1.5 m at a depth of 15 m outside of the estuary and 0.2 m or less in the shallow region of the estuary. The total numbers of triangular elements and nodes were 20,677 and 10,829, respectively. The time step used for the external mode was 1.2 s and the ratio of the internal mode to the external mode was 10.

[13] The model was driven by tidal elevation consisting of five major tidal constituents (M_2, S_2, N_2, K_1, and O_1) at the open boundary connecting to the inner shelf. To avoid artificial numerical modes created by a sudden impulse from

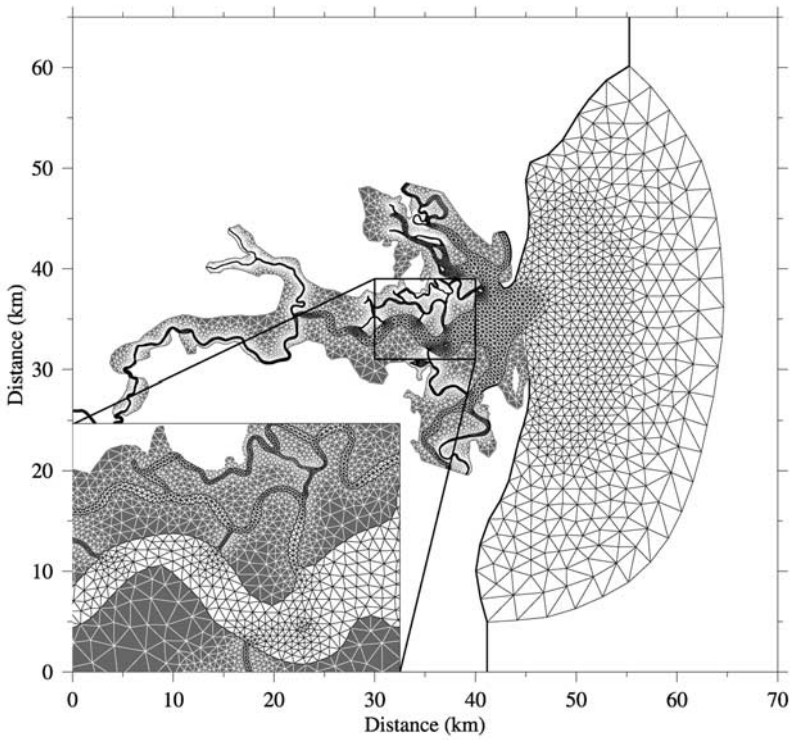

Figure 2. Unstructured triangular grid of FVCOM in the Satilla River Estuary. Total number of elements and nodes are 20,677 and 10,829, respectively. Horizontal resolution (estimated by the longest length of a triangle) varies from 40–100 m in tidal creeks and main channels to 2.5 km near the open boundary over the inner shelf.

the initial condition [*Chen et al.*, 2006a], the tidal forcing was ramped up from zero to its full value over two M_2 tidal cycles. The tidal simulation results were compared with surface elevation data measured at seven sites, current velocity data at two moorings, and ship-towed ADCP data collected along the main channel. The surface elevation and moored current meter data were provided by J. Blanton (Skidaway Institution of Oceanography, SKIO). The ADCP data were collected from two independent surveys: one on 11 March 1999 by H. Seim (University of North Carolina, UNC) [*Seim et al.*, 2006], and the other on 17–18 November 2004 by C. Li (Louisiana State University, LSU).

[14] Long-term hydrographic and current measurements have demonstrated that the Satilla River Estuary is a salinity controlling system [*Blanton et al.*, 1999]. The spatial and temporal variability of the salinity is a result of mixing between the freshwater discharged from the upstream and saltwater intruding from the inner shelf of the SAB [*Zheng et al.*, 2003a]. A numerical experiment was conducted to simulate the along-estuary distribution of salinity, which was initialized using the observed salinity data from the hydrographic survey at neap tide on 7 April 1995 and obtained by running the model for nine consecutive days. The model results were output and compared with the salinity data measured at the spring tide on 15 April 1995. This experiment was designed to examine the capability of FVCOM to reproduce the salinity field for a given realistic initial condition.

[15] A Lagrangian particle tracking experiment was conducted to study the water exchange process over the estuarine tidal-creek salt-marsh complex. Particles were released at different phases of a M_2 tidal cycle in the main channel and over an intertidal salt marsh. All particles were neutrally buoyant, tracked in the model space (x, y, σ). The trajectories of the particles were then converted back to the Cartesian coordinate space (x, y, z). This method avoids the interpolation errors caused by repeated transformations from σ- to z-coordinates. A detailed description of the 3D Lagrangian tracking model with a full consideration of strong nonlinearity was given in the FVCOM user manual [*Chen et al.*, 2006a].

[16] We also examined the impact of the surface wind on currents and particle movement in Satilla River Estuary. The wind-forcing is taken from a hindcast run of the fifth-generation mesoscale Meteorological Model (MM5) [*Dudhia et al.*, 2003; *Chen et al.*, 2005], which was set up for the SAB area including Georgia and South Carolina estuarine regions (http://fvcom.smast.umassd.edu/research_projects/SATILLA/home.html). Except near the mouth area, no significant difference was found inside the estuary for the cases with and without wind-forcing. See our Satilla River Estuary website for a detailed discussion for the role of wind-forcing in the Satilla River Estuary.

3. Tidal Simulation and Residual Flow

[17] With the wet/dry point treatment, FVCOM was robust in resolving the 3D flooding/drying process over the estuarine tidal-creek salt-marsh complex in the Satilla River Estuary. During the flood tidal period, the coastal water flowed from the inner shelf into the main channels, moved around islands/barriers and then split into tidal

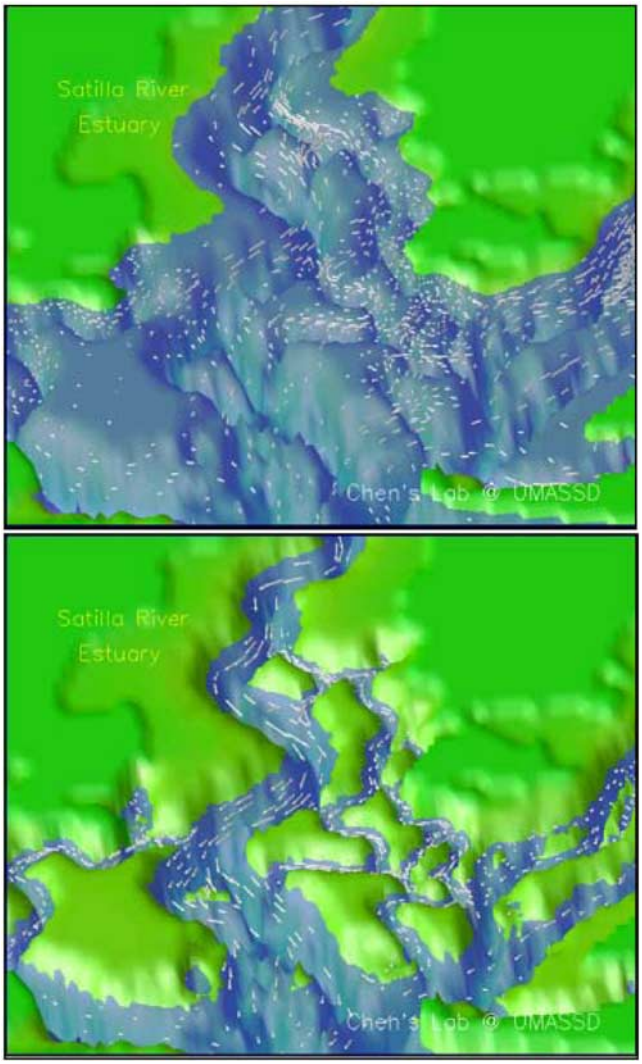

Figure 3. A 3D view of the flooding and drying process in the downstream region of the Satilla River Estuary. The images were taken after the maximum flood and ebb tidal currents.

creeks (Figure 3a). The intertidal salt marsh areas were flooded by the incoming water from the main channels and also from the tidal creeks. In turn, during the ebb tidal period, the water over the salt marsh was first drained into tidal creeks and then into the main channel, before flowing out to the inner shelf (Figure 3b). The flooded area of the intertidal salt marsh varied remarkably with the fortnightly spring-neap period of the tidal motion. In general, about 80–90% of the salt marsh was flooded twice per day. During the spring tide, water can cover the entire salt marsh.

[18] The timing of high water varied with the distance from the shelf, up to greater than 1 h between the mouth and head of the river. The high and low waters defined in this study referred to the maximum and minimum mean water levels over the main channel. The phase difference was evident in the distribution of tidal currents. At high water, for example, the tidal currents were dominated by an inflow in the upstream part of the main channel when the flow was outward at the open boundary on the inner shelf (Figure 4a). At low water, the estuarine water in the upstream area moved seaward, but a relatively strong inflow had already occurred at the mouth, which brought a significant amount of seawater into the estuary including the tidal creeks (Figure 4b). As a result, the tidal currents feature a divergence field at high water and a convergence field at low water. Similar spatial variations were also evident at a transition of ebb-flood or flood-ebb tidal currents.

[19] The model-predicted amplitudes and phases of the tidal elevation were validated by comparison with tidal constants estimated by bottom pressure data at seven sites shown in Figure 1. These measurements covered a 70-d period from 2 January to 13 March 1999. The observations showed that the M_2 tidal elevation gradually increased from 94.7 cm at site 1 to 99.4 cm at site 4, dropped to 96.0 cm at site 5 (close to the upstream end of the main channel) and then changed to 96.4 cm at site 6 (in the right branch) and 92.2 cm at site 7 (in the left branch). This longitudinal variation in M_2 elevation was reproduced by FVCOM (Figure 5). The disagreement between model-predicted and observed M_2 tidal amplitudes was within the observational error. Similar agreement was also found for other semidiurnal (S_2 and N_2) and diurnal (K_1 and O_1) tidal constituents (Figure 5). The phase of the observed tidal elevation varied significantly along the estuary. The phase difference between site 1 and site 6 or 7 was $\sim 34^\circ$ for M_2, $\sim 50^\circ$ for S_2, $\sim 48^\circ$ for N_2, $\sim 27^\circ$ for K_1 and $\sim 21^\circ$ for O_1. The model accurately captured the longitudinal trend of the phase delay for all five major tidal constituents. The model-predicted tidal phases agreed well with the observations at sites 1–4, but slightly overestimated the phase delay at site 5 (close to the upstream end of the main channel) and at sites 6 and 7 in the two branches. These numerical experiment showed that the model-predicted tidal phase in the upstream area was sensitive to the bottom roughness (z_o) selected in the model. In the Satilla River Estuary, the sediment content was quite different in the upstream and downstream regions [*Zheng et al.*, 2003b], so that the value of z_o was thought to vary widely in space along the main channel. Since the tidal phase is related to bottom friction, it was not a surprise that the model accurately captured the amplitude but with some minor error in phase.

[20] Two moorings were deployed at site A (81°32.28′W, 30°59.58′N) and site E (81°30.84′W, 30°59.16′N) in the Satilla River Estuary between 26 March and 27 April 1999. A comparison between model-predicted and observed tidal current ellipses was made at these two sites and the results showed a good agreement in the major and minor axes and orientation of the ellipses, and phase for all five major tidal constituents (Figure 6). For example, the maximum difference in the M_2 tidal current ellipse was 1.8 cm/s at site A and 2.3 cm/s at site E in major axes, with a standard deviation of 0.7 cm/s. This value was within the measurement uncertainty of 0.8–1 cm/s. The model predicted phase showed a relatively large bias at site A (Table 1), which was probably related to the parameterization of bottom roughness used in this model since the phase is sensitive to bottom friction.

[21] In the Satilla River Estuary, the residual currents, which were defined as the averaged subtidal currents de-tided using Foreman's harmonic analysis program, were characterized by multiple eddies along the curved estuarine channels, around the shallow sounds and coastal headland

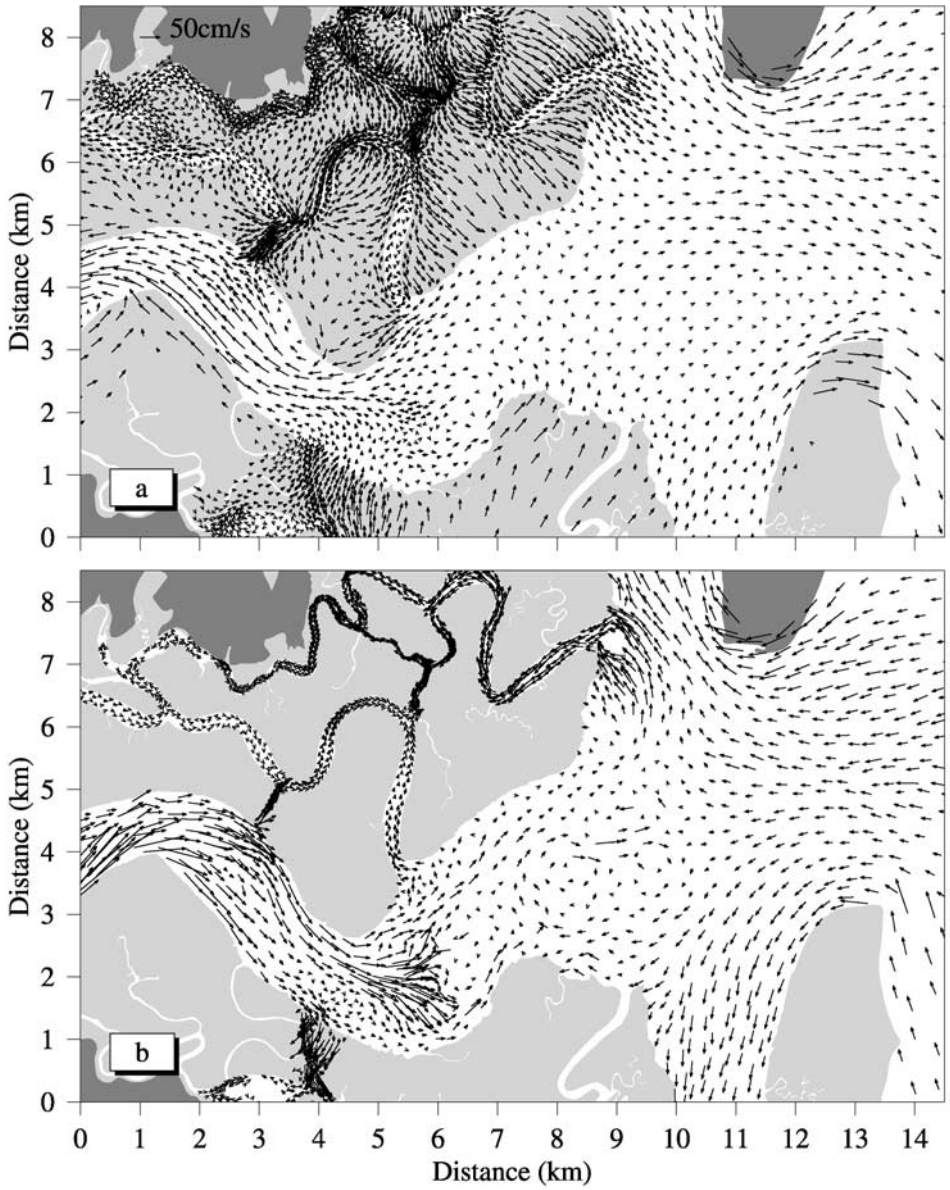

Figure 4. Distribution of the near-surface currents during (a) flood and (b) ebb tides for the case with only tidal forcing.

(Figure 7). All convex coastal areas in the estuary featured a pair of cyclonic and anticyclonic residual eddies. The maximum magnitude of an eddy swirl current exceeded 10 cm/s. At the estuary mouth, a pair of eddies were found near both the northern and southern headlands, which were formed by tidal flushing along the meandering channel [*Li et al.*, 2008]. In the wide interior region, bathymetry was very complex: the shallower area is surrounded by "deep" water passages. Tidal flushing over the bottom topography generated eddies over the shallower area. Therefore the Satilla River Estuary is eddy-featured, in sharp contrast to flows in highly idealized estuarine models with simple bathymetry.

[22] The model-predicted residual eddy field was in good agreement with the de-tided flow field from the towed-ADCP measurements made on 11 March 1999 by Seim and also on 17–18 November 2004 by Li. Removing tidal signals with a spatially dependent least squares fitting method, *Seim et al.* [2006] detected a pair of residual eddies on the sides of a convex area of the Satilla River Estuary: anticyclonic on the left and cyclonic on the right. Figure 8 shows a comparison between FVCOM-predicted and observed residual flow fields de-tided in the ADCP survey area on 11, 18, and 20 March 1999. The residual eddies, detected with the ADCP measurements, were captured by FVCOM. The model-predicted residual eddy currents are asymmetrically distributed across the estuary. In the anticyclonic eddy, the currents were much stronger on the northern side than on the southern side. In the cyclonic eddy, however, the distribution was opposite. Although the ADCP survey did not cover the entire area of the eddy field, it did show strong anticyclonic and cyclonic currents on the northern and southern sides, respec-

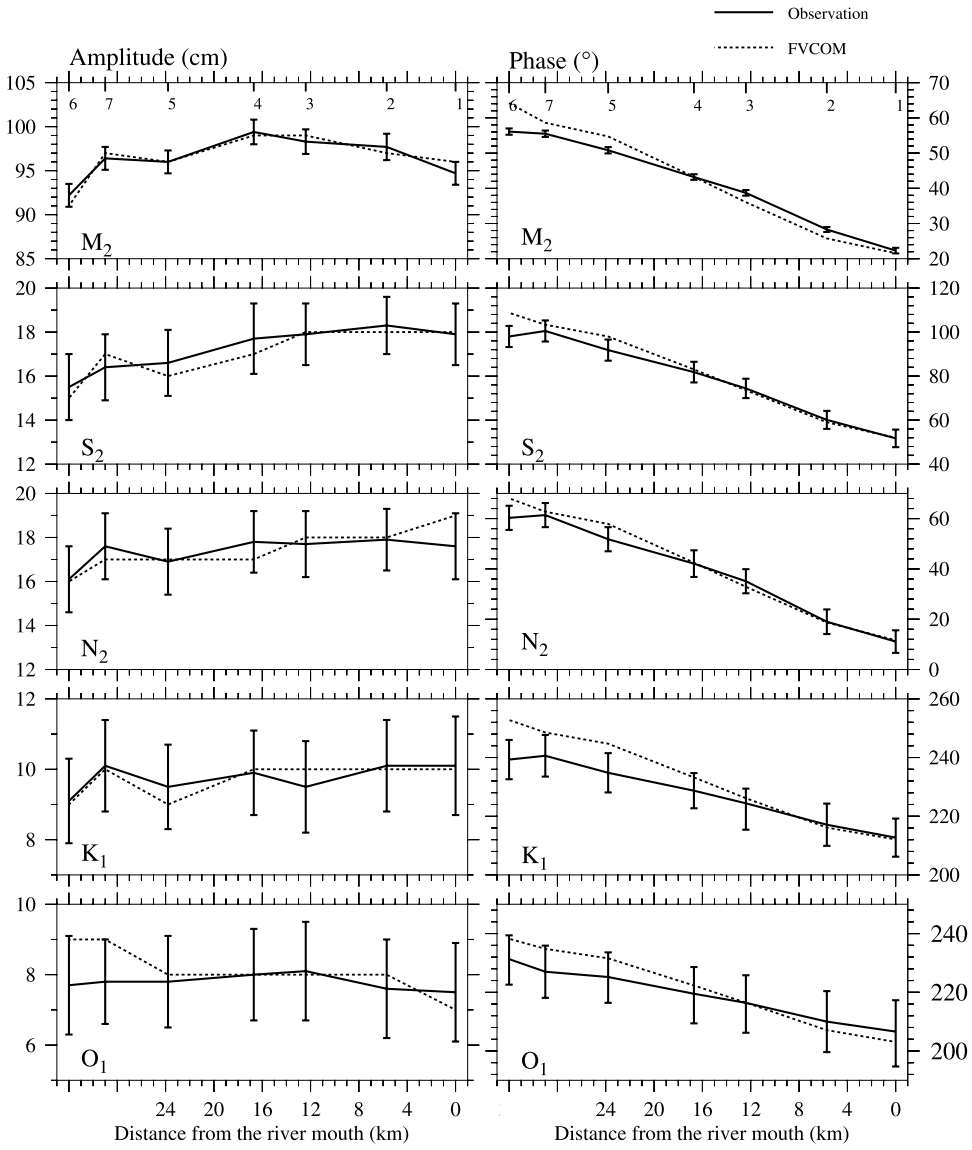

Figure 5. Comparisons of model-predicted and observed amplitudes (left) and phases (right) of M_2, S_2, N_2, K_1, and O_1 tidal constituents at the measurement sites numbered 1 to 7. The distance shown in the lower axis was calculated relative to Site 1.

tively. The model also predicted an eddy pair in the convex region of the Satilla River Estuary near the ADCP survey area shown in Figure 8. These patterns were consistent with the residual flow de-tided from the 17–18 November 2004 towed-ADCP survey data (Figure 9). The agreement in pattern and magnitude between model-predicted and observed residual flow fields suggests that the model was sufficiently robust to resolve the residual eddy feature in a complex geometry estuary.

4. Salinity Simulation

[23] An experiment was conducted to examine the capability of FVCOM to simulate the spatial and temporal variability of salinity in the Satilla River Estuary. The simulation was carried out through a "hot start" approach with initial fields of model-predicted tidal elevation and currents, river discharge rate recorded at the upstream end and water salinity measured on 7 April 1995. The 7 April 1995 hydrographic survey was carried out at mean low water. The model was run prognostically for 1 month and the model output salinity was compared with the salinity measured along an estuarine transect from 6:36–10:05 AM on 15 April 1999 (around mean high water) and from 13:57–17:17 PM on 15 April 1999 (around mean low water). The model output was sampled by following the survey tracks. We also compared the model-predicted salinity with an observed time series recorded at an anchored site over a tidal cycle on 16 April 1999.

[24] On 15 April observations around mean high water showed that salt water occupied almost the entire main channel, with a value ranging from 26 psu at the estuary mouth to ~1.0 psu at the head where the river splits into two branches (Figure 10a). The salt water was well mixed

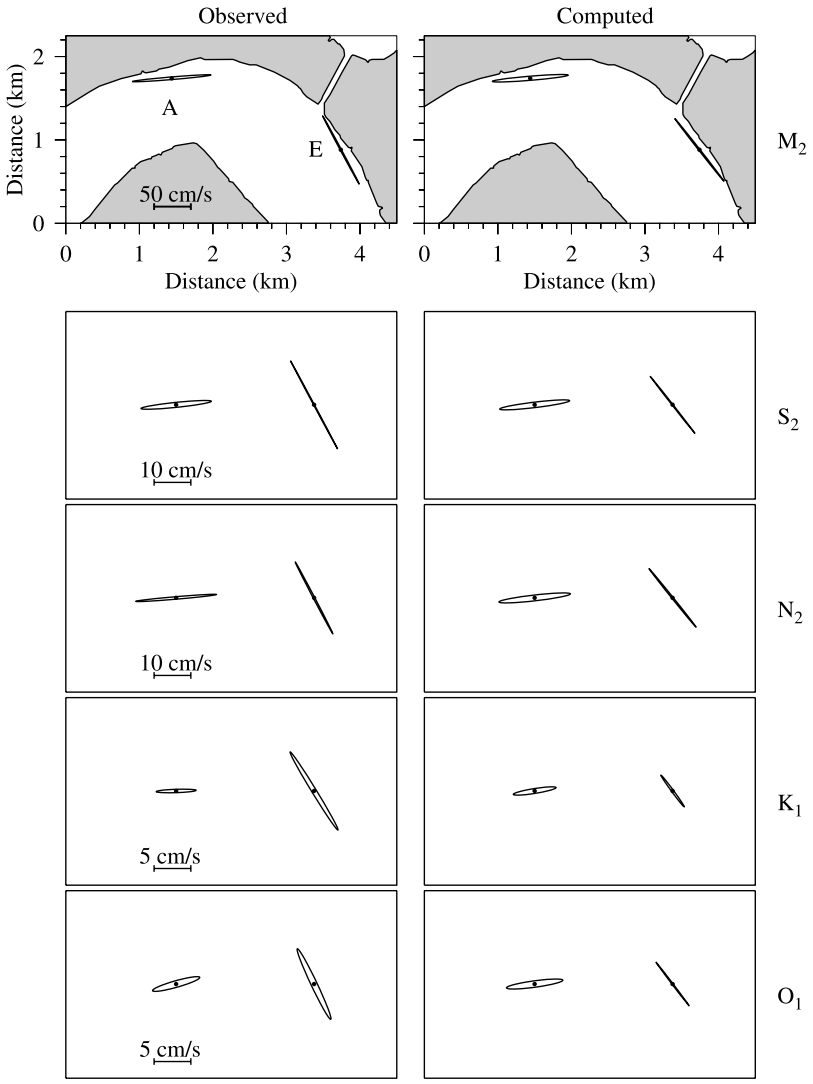

Figure 6. Comparisons of observed (left) and model-predicted (right) tidal current ellipses of M_2, S_2, N_2, K_1, and O_1 constituents at Sites A and E.

vertically, with the largest longitudinal gradient located ~17–21 km upstream from the estuary mouth (around the 5th and 6th CTD stations [counted from the estuary mouth]). Around mean low water, the measurements taken during the neap tidal cycle showed that salt water was significantly withdrawn seaward (Figure 11a). The freshwater boundary, which was located ~30 km upstream from the estuary mouth during the spring tidal cycle, moved

Table 1. Comparison Between Model-Predicted and Observed Tidal Current Ellipses at Two Measurement Sites A and B

		Umajor, cm/s		Uminor, cm/s		Orientation, deg		Phase, deg	
		Observed	FVCOM	Observed	FVCOM	Observed	FVCOM	Observed	FVCOM
Site A	M_2	53.4 ± 0.77	51.70	−1.6 ± 0.47	−2.48	4.2 ± 0.5	4.2	156.7 ± 0.8	154.2
	S_2	9.6 ± 0.78	9.55	−0.6 ± 0.51	−0.66	5.2 ± 3.6	6.1	203.0 ± 4.7	195.6
	N_2	11 ± 0.88	9.77	−0.3 ± 0.47	−0.70	4.3 ± 2.6	5.7	142.4 ± 4.1	151.1
	K_1	2.8 ± 0.84	2.93	0.1 ± 0.64	0.29	5.5 ± 14.1	8.0	326.4 ± 21.2	319.6
	O_1	3.3 ± 0.96	3.86	−0.4 ± 0.62	−0.39	14.0 ± 11.7	6.8	2.9 ± 16.9	26.3
Site E	M_2	47.8 ± 0.95	50.18	0.8 ± 0.40	0.87	121.3 ± 0.5	131.6	150.0 ± 1.2	150.6
	S_2	12.6 ± 1.02	9.09	−0.1 ± 0.44	−0.12	121.2 ± 2.1	131.6	16.4 ± 5	11.5
	N_2	10 ± 0.94	9.47	0.2 ± 0.42	0.18	120.7 ± 2.6	132.3	309 ± 5.9	326.9
	K_1	5.9 ± 0.96	2.47	−0.5 ± 0.53	−1.32	128.3 ± 4.7	129.7	98.8 ± 9.9	119.2
	O_1	4.9 ± 1.04	3.43	0.4 ± 0.53	0.07	118.3 ± 6.7	130.7	150.5 ± 15.1	139.5

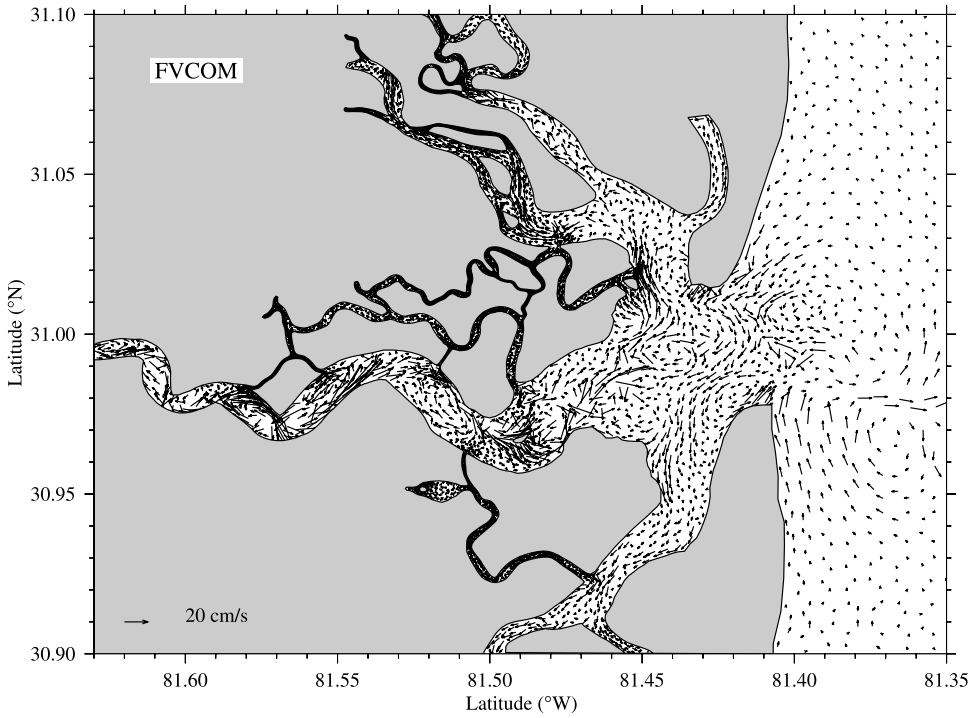

Figure 7. Distribution of the vertically averaged tidal residual current vectors de-tided from the 40-d model run for the case with only tidal forcing.

seaward over a distance of 12 km. During this period, the salinity level in the estuary dropped to 18 psu, about 9 psu lower than that observed during the spring tide.

[25] The observed longitudinal distributions of salinity during the spring and neap tidal cycles were captured by FVCOM with the inclusion of the flooding/drying process. The model reproduced the same fortnightly variability and longitudinal salinity distribution over the spring-neap tidal cycle. The model-predicted location and intensity of the salinity front and the salinity values at spring and neap tides are consistent with the observations (Figures 9b and 10b). A slight model-data difference was noted in the two upstream branches. Because no salinity measurements were taken in the two upstream branches on 7 April 1999, the initial model salinity was simply specified as zero everywhere in both upstream river branches and in the salt marsh area. This assumption seems to underestimate the salinity level of estuary water covering the salt marsh area connecting the two upstream river branches.

[26] FVCOM also captured the salinity variability over tidal cycles at an anchor site where a salinity time series was recorded (Figure 12). The observations showed that the salinity dropped from 16 psu to 2 psu during the ebb tide and then increased to 20 psu during flood tide. This temporal variation was reasonably reproduced by the model. The model-predicted timing of the minimum salinity was in good agreement with the observations, while the model seemed to underestimate the salinity in the late phase of the flood tide. The high salinity value observed near the flood-ebb transition was probably caused by salt water flowing from the salt marsh. Since no measurements were made over the salt marsh, the salinity over the intertidal marsh areas were specified as zero at initial time in the model, which was probably one of the reasons that caused the model's underestimation of the salinity level during the flood phase.

5. FVCOM and ECOM-si Comparison

[27] FVCOM was originally developed to simulate the flooding/drying process in the Satilla River Estuary because of the failure of ECOM-si in resolving the complex geometry of the tidal creeks, islands and barriers. Tidal creeks in the Satilla River Estuary function as a network of waterways to link the main channel to surrounding waters including intertidal salt marshes. As a typical structured-grid finite difference model, the curvilinear grid used in the Satilla River Estuary, ECOM-si could not properly resolve the irregularly shaped tidal creeks. That model treated the creeks as part of the intertidal zone that only filled during flood tide [*Zheng et al.*, 2003a]. This simplification provided a reasonable simulation of tidal currents and salinity in the main channel, but failed to capture the correct kinematics of water exchange over the estuary-intertidal salt marsh complex.

[28] To illustrate the usefulness of an unstructured-grid model to study estuaries with complex shape and bathymetry, we compared the FVCOM-derived flooding/drying process with results from the previous Satilla River Estuary ECOM-si study. During flood tide, FVCOM showed that the salt marsh was flushed by water from both the main channel and the tidal creeks (Figure 13a). The tidal currents varied significantly in tidal creeks and over the salt marsh. Water drained from the salt marsh into tidal creeks and then

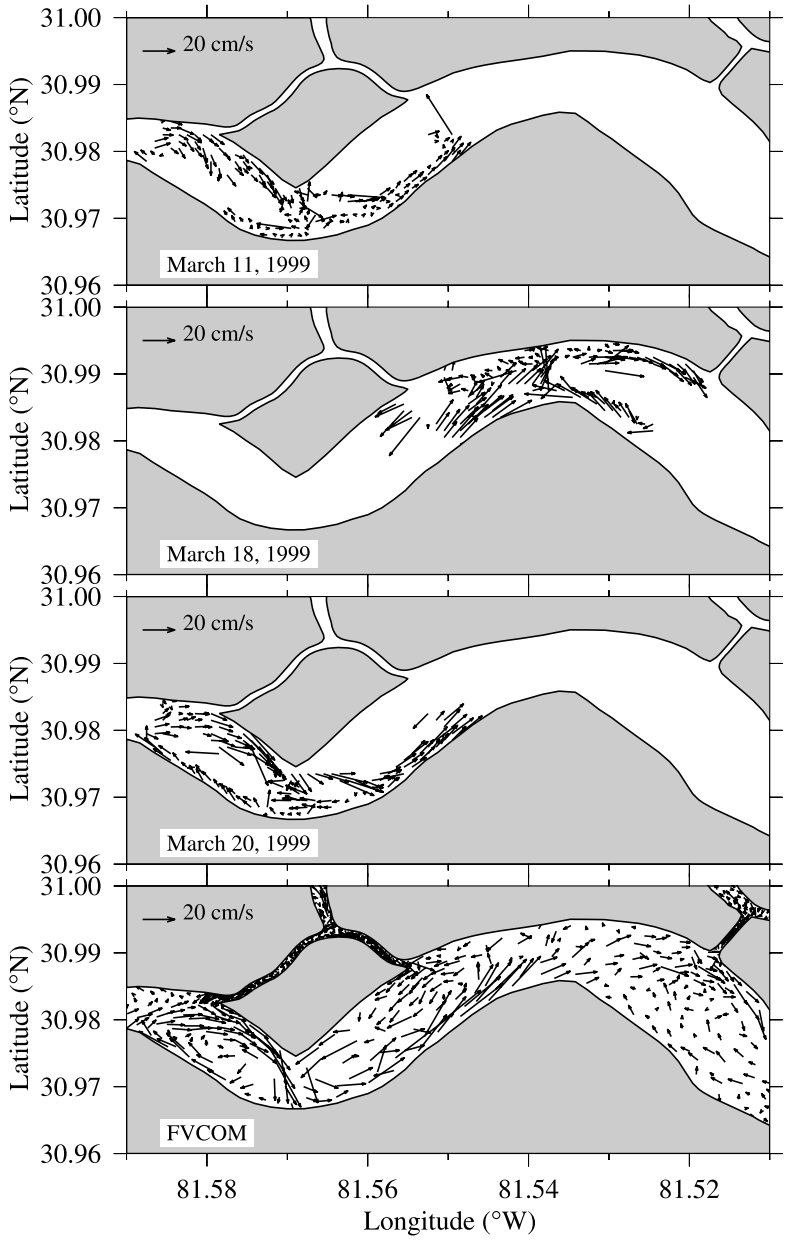

Figure 8. Comparison of (top) observed and model-predicted residual flow field in the Satilla River Estuary. The observed residual currents on 18 and 20 March 1999 were processed using Chunyan Li's ADCP de-tided program.

flowed into the upstream marsh areas. During ebb tide, FVCOM showed that the water covering the intertidal salt marsh drained back to the main channel through multiple passages. Portions of the water flowed directly to the estuary through their boundaries, but the remaining water first drained back into the tidal creeks before flowing into the estuary (Figure 14a). At mean low water, all water covering the salt marsh had moved back into the tidal creeks and the estuary.

[29] Failing to resolve the tidal creeks, the Satilla River Estuary ECOM-si model predicted a completely different water transport process over the estuary-intertidal salt marsh complex. During flood tide, this model showed that the salt marsh was flooded by relatively spatially uniform tidal currents from both the main channel and the inflow from surrounding sounds (Figure 13b). In this model, the salt marsh was just like a box with boundaries connected to the estuary and sounds. In such a box model system, the salt marsh was flooded only through the water exchange between its boundaries. During ebb tide, water on the salt marsh moved back to the estuary only through the marsh-estuary boundary. This draining process was much slower than that predicted by FVCOM. At mean low water, there was still a significant amount of water covering the salt marsh area connected to the main channel (Figure 14b). Because of the tidal phase delay between downstream and

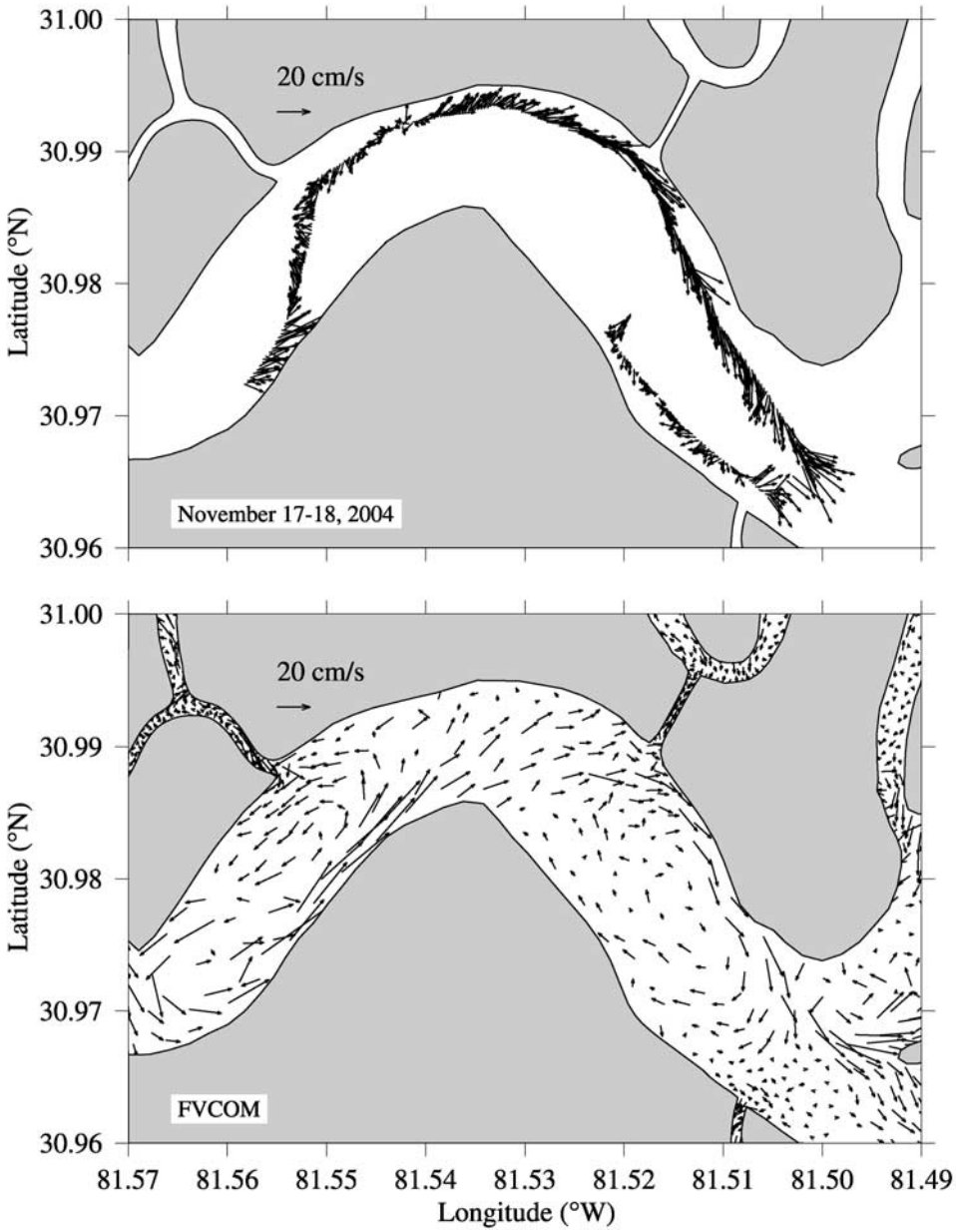

Figure 9. Comparison of (top) observed and model-predicted residual flow field in the 17–18 November 2004 ADCP survey area from the Satilla River Estuary. The ADCP field survey was supported by the Georgia Sea Grant Program led by C. Li and C. Chen.

upstream areas, the water had already flushed onto the salt marsh area in the downstream region close to the estuary mouth before the upstream salt marsh area was completely drained. Therefore in this ECOM-si simulation, the salt marsh area was never completely drained during ebb tide.

[30] A Lagrangian particle tracking experiment was conducted to examine how tidal creeks affect the water movement in the predicted flow field from the Satilla River Estuary FVCOM and ECOM-si models. Driven only by the M_2 tidal forcing, we released particles inside the estuary and salt marshes during different phases of tidal cycles. No matter when and where the particles were released, the two models predicted significantly different particle trajectories. Examples are shown in Figures 15 and 16 for a selected particle release over the salt marsh at high and low water, respectively.

[31] Releasing a particle near the edge of the salt marsh connected to the main channel at high water (Figure 15), FVCOM showed that the particle turned cyclonically and moved to the interior of the estuary during the first ebb tidal period. This particle flowed back to the salt marsh through the tidal creek during flood tide and then back and forth between the interior of the estuary and the edge of the marsh in the tidal creek over additional tidal cycles. After four tidal cycles, it was located at the northern edge of the salt marsh connected to the tidal creek. For the same case, ECOM-si showed that the particle moved back and forth following

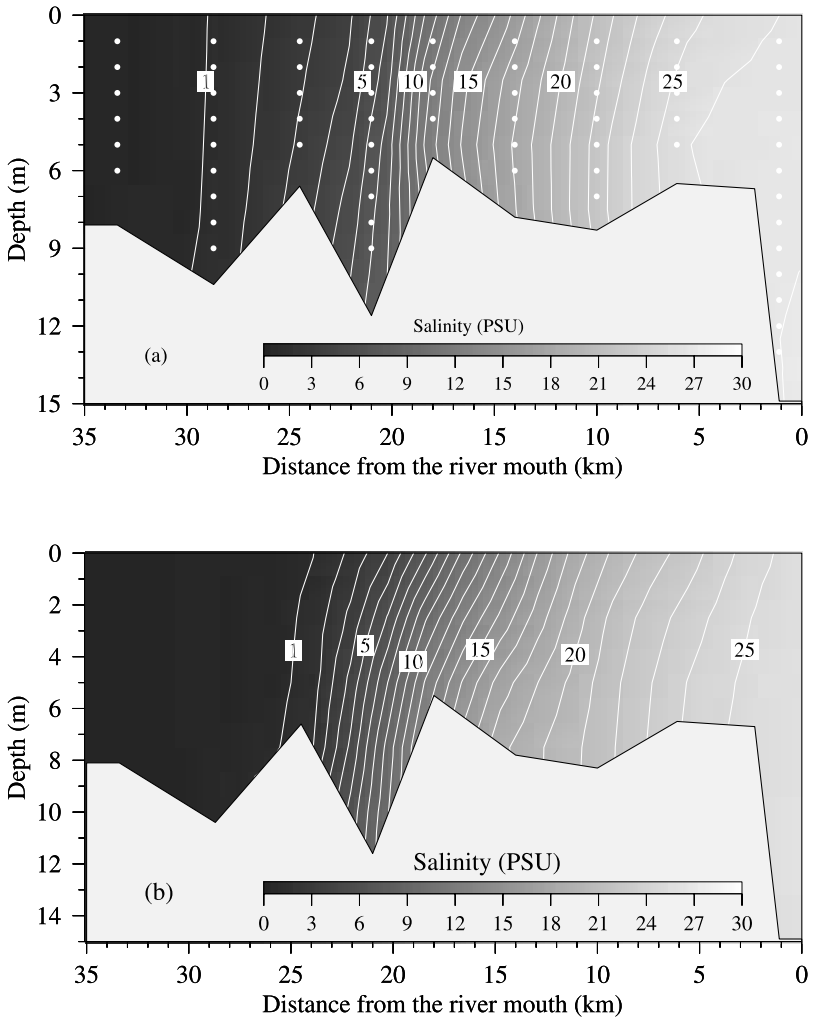

Figure 10. Comparison of the observed (top) and model-predicted (bottom) along-estuary salinity distributions at mean high water on 15 April 1999.

parallel trajectories between the salt marsh and the estuary. After four tidal cycles, this particle moved to an upstream location inside the main channel.

[32] Releasing a particle at a location over the salt marsh connected to the tidal creek at mean low water (Figure 16), FVCOM showed that the particle moved into the tidal creek and oscillated back and forth between the salt marsh and interior of the estuary over several tidal cycles. After five tidal cycles, it arrived at a location near the estuary mouth. For the same case, ECOM-si showed that the particle moved back and forth within the salt marsh in the first four tidal cycles, then drifted to the northern region and stayed at a location near the northern headland of the estuary mouth.

[33] The trajectories of a group of particles released over the salt marsh at mean high and low water are shown in Figures 17 and 18, respectively. For particles released at mean high water (Figure 17), FVCOM showed that the particles moved into the surrounding tidal creek and to the interior of the estuary during the first tidal cycle, split into two separate patches in the second tidal cycle, and then dispersed over the marsh area after the third tidal cycle. At the end of fifth tidal cycle, the particles had already spread over a wide area, ranging from the upstream to the northern estuary channels connected to the estuary mouth. ECOM-si showed that particles moved back and forth as a single patch between the marsh and interior of the estuary in the first four cycles and then split into two patches in the fifth tidal cycle.

[34] For particles released at mean low water (Figure 18), FVCOM showed that particles moved periodically along the axis parallel to the main channel over several tidal cycles and dispersed widely over the distance between the head of the estuary and inner shelf by the fifth tidal cycle. ECOM-si showed that particles moved mainly in the marsh during the first four tidal cycles, with completely different trajectories from those predicted by FVCOM.

[35] The FVCOM and ECOM-si comparison in the Satilla River Estuary indicates that the interpretation of the results from the structured-grid Satilla River Estuary ECOM-si model for a complex estuary, particularly for the study of exchange of water over estuarine wetlands, should be approached cautiously. Even with an accurate wet/dry point

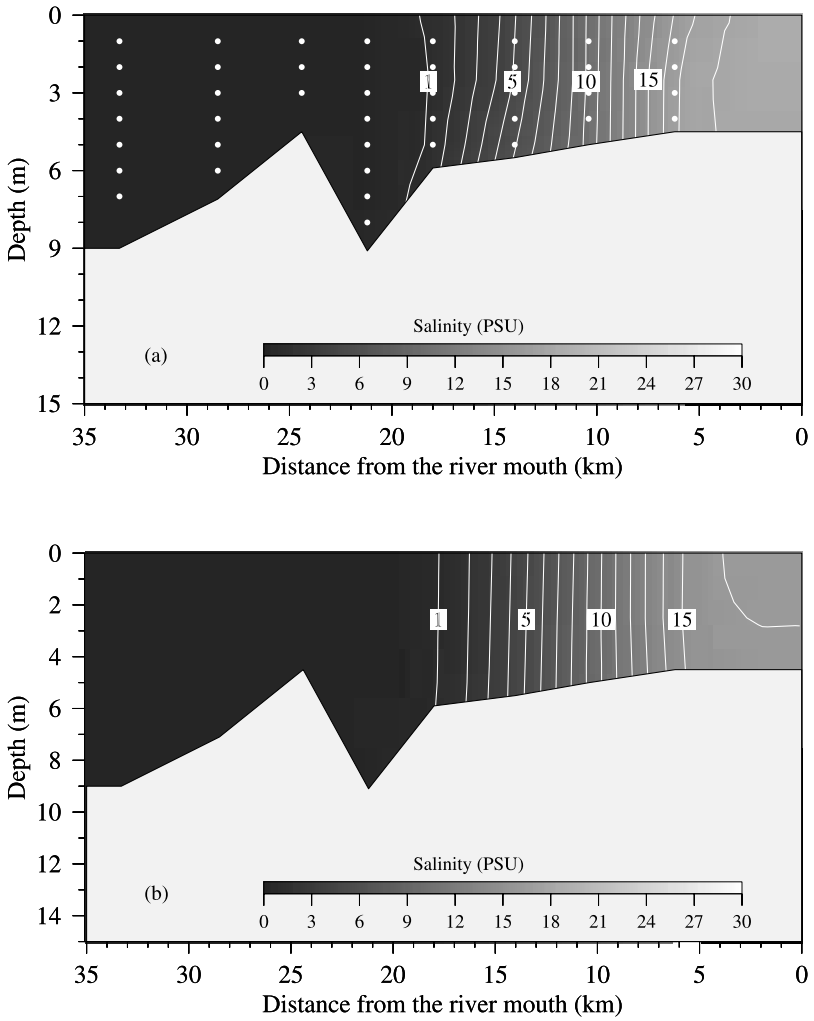

Figure 11. Comparison of the (top) observed and (bottom) model-predicted along-estuary salinity distribution at mean low water on 15 April 1999.

treatment, failure to resolve the complex geometry of an estuary can result in an incorrect prediction of the water exchange.

6. Discussion

[36] The model experiments show that geometric flexibility in FVCOM is robust enough to simulate the marsh flooding/drying process and thus produce a more realistic prediction of the water exchange over the estuarine tidal-creek salt-marsh complex in the Satilla River Estuary. The comparison between FVCOM and ECOM-si provides a general review and critique of the inherent limits associated with the application of a structured-grid model to a complex estuarine system. Dynamics and kinematics in a realistic estuary system are much more complex than what we recognized from either traditional conceptual (idealized) estuarine systems or limited field measurements. Both field measurements and modeling indicate that complex estuaries are characterized by multiscale flow features and dynamics with significant influences from local geometry and bathymetry. Process-oriented experiments conducted in this study have demonstrated a critical need for an unstructured-grid model with flexibility in geometric fitting and horizontal resolution to resolve the complex fine structure of an estuary. Failure to resolve this geometrically generated and controlled fine structure can result in an unrealistic water exchange process and thus produce incorrect residence/flushing time estimates as well as miss or mislocate retention zones in estuaries, all of which are critical for advanced estuarine ecosystem studies [*Alber and Sheldon*, 1999].

[37] Tidal flushing along the meandering Satilla River Estuary and changes in bathymetry produced multiple residual eddies. In our previous studies, we found that eddies in different regions were driven by multiscale physical processes related to tidal rectification over bottom topography, inertial effects around the curving coastline, asymmetry of tidal currents over tidal cycles, and nonlinear interactions between tidal and buoyancy flows over complex bathymetry [*Zheng et al.*, 2003a]. Recently, *Li et al.* [2008] used a simple idealized estuary model to explore the dominant physical mechanism for eddy formation in the Satilla River Estuary. The major finding from this simple

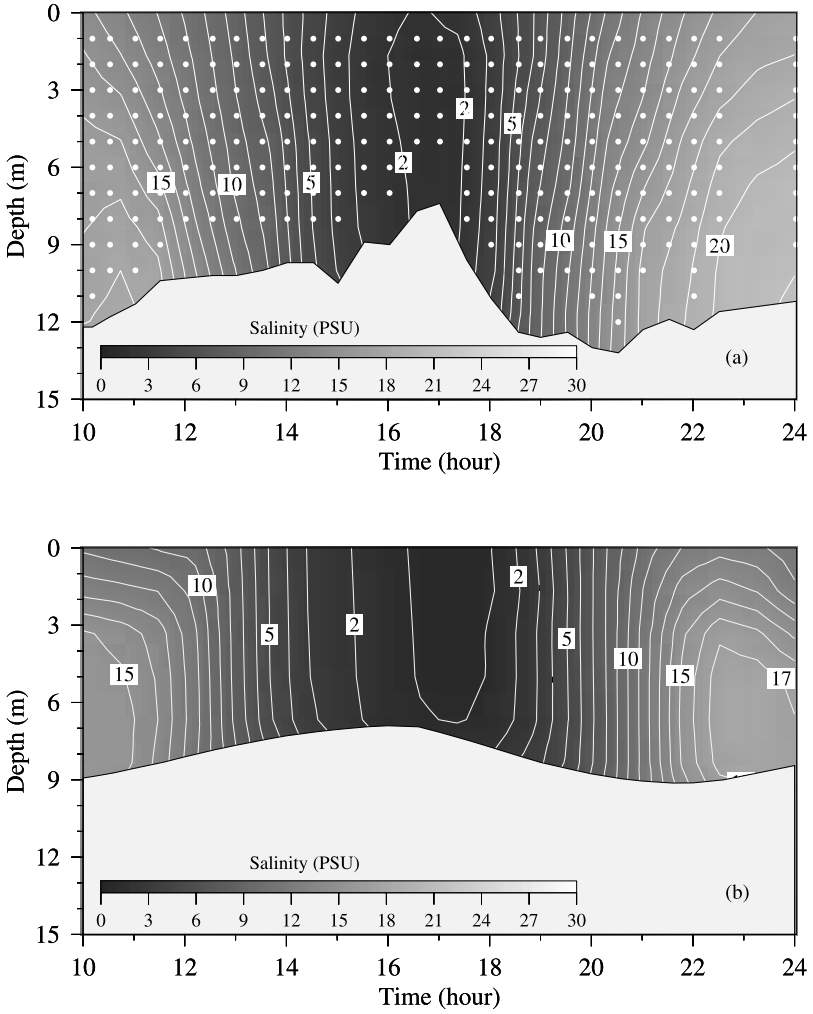

Figure 12. Comparison of the observed (top) and model-predicted (bottom) salinity at the anchor site shown in Figure 1. During the measurement, the surface was selected as the origin of the coordinate (z = 0). The shadow area indicates the temporal variation of sea elevation rather than real bottom topography. Filled circles in the upper panel were the measurement depths.

barotropic model is that the asymmetry of advection is a major contributor to the generation of residual eddies around a curved section of an estuary. A detailed discussion of this study is given by *Li et al.* [2008].

[38] It should be pointed out that the intermodel comparison presented here is aimed at examining the impact of tidal creeks on the flooding/drying process (or water exchange) over the estuarine tidal-creek salt-marsh complex. For this purpose, FVCOM and ECOM-si were chosen as examples of two existing Satilla River Estuary models with and without tidal creeks, islands and barriers. The comparison is discussed to emphasize the importance of resolving the irregular geometry of an estuary in realistic applications. If the comparison is aimed at validating the capability of unstructured- and structured-grid models to resolve a complex estuarine system, then the numerical experiments should be made with the same horizontal resolution. In the present case, this would require a significant increase in the Satilla River Estuary ECOM-si horizontal grid resolution, which would significantly increase the computational effort, making it more costly to run than the Satilla River Estuary FVCOM. This highlights the advantage of an unstructured-grid model which can allow high-resolutions in areas of interest while maintaining minimum resolution in areas of less importance, thereby making the overall computation efficient. Detailed discussions of the role of grid resolution in comparisons of FVCOM with structured-grid models in other coastal settings and idealized test problems are presented by *Chen et al.* [2007] with an emphasis on the importance of coastline fitting and by *Huang et al.* [2008] with discussions on properties of numerical dispersion, damping, and performance of the structured-grid ROMS and unstructured-grid FVCOM models.

7. Summary

[39] By resolving the complex geometry of tidal creeks, narrow branches, islands and barriers, the unstructured-grid

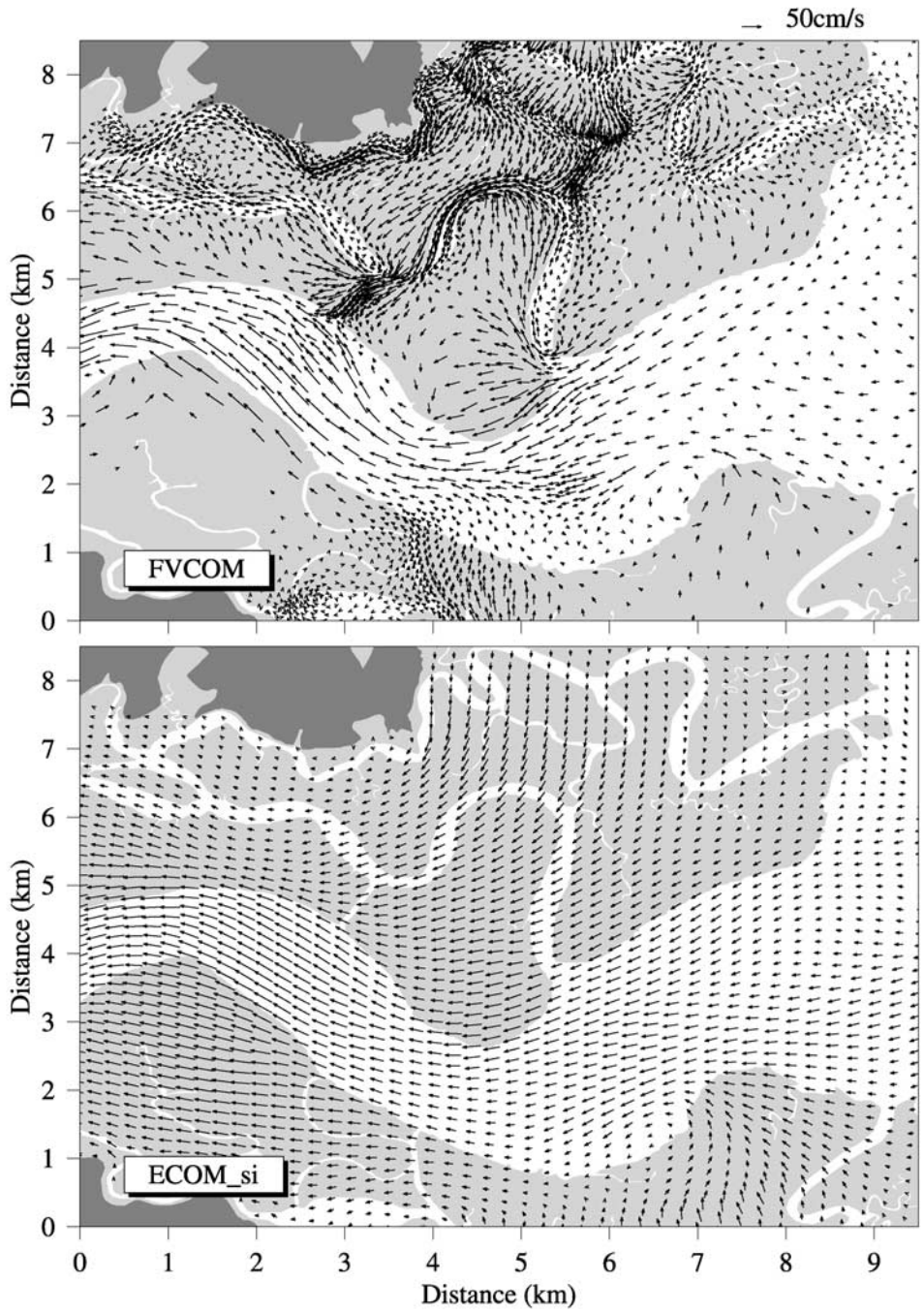

Figure 13. Comparison of snap shots of the near-surface current in a selected region of the Satilla River Estuary during flood tide for (top) FVCOM and (bottom) ECOM-si models.

FVCOM produced a realistic tidal flooding/drying process in the Satilla River Estuary and simulated the temporal and spatial distributions of the amplitude and phase of the tides and salinity observed at both the mooring sites and along hydrographic transects. The model-predicted residual flow field is characterized with multiscale eddies around curvatures, islands, headlands and entrances to tidal creeks. The existence of these residual eddies in this estuary is supported by ship-towed ADCP measurements.

[40] An intermodel comparison between the existing Satilla River Estuary FVCOM and ECOM-si suggests that failure to resolve the geometric ''fine structure'' of an estuary can lead to the prediction of an unrealistic water exchange process over the estuarine intertidal salt-marsh complex. Since the current dynamics in estuaries are generally geometrically controlled, it is critical to apply a mass-conservative unstructured-grid model to realistic estuarine studies.

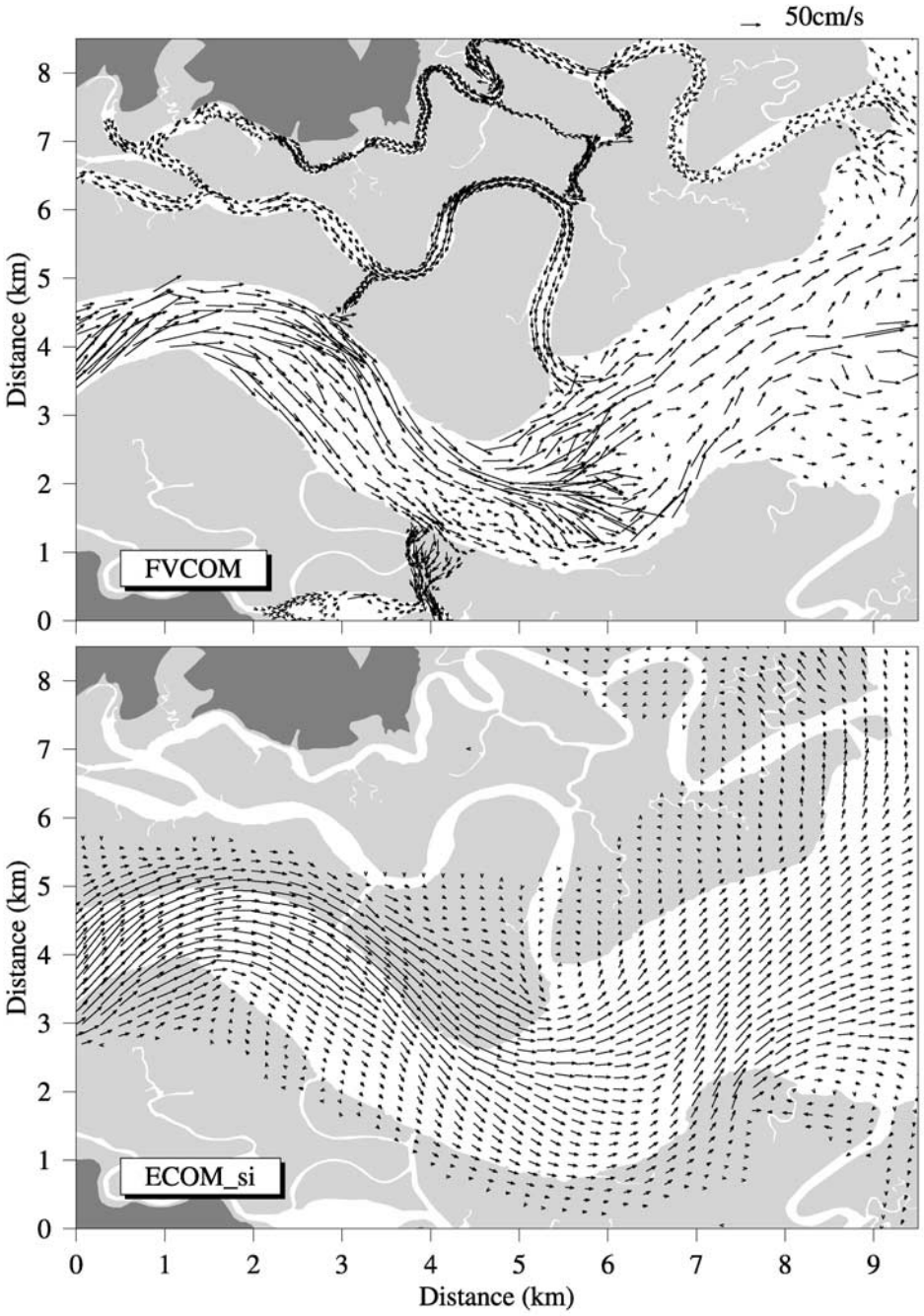

Figure 14. Comparison of snap shots of the near-surface current in a selected region of the Satilla River Estuary during ebb tide for (top) FVCOM and (bottom) ECOM-si models.

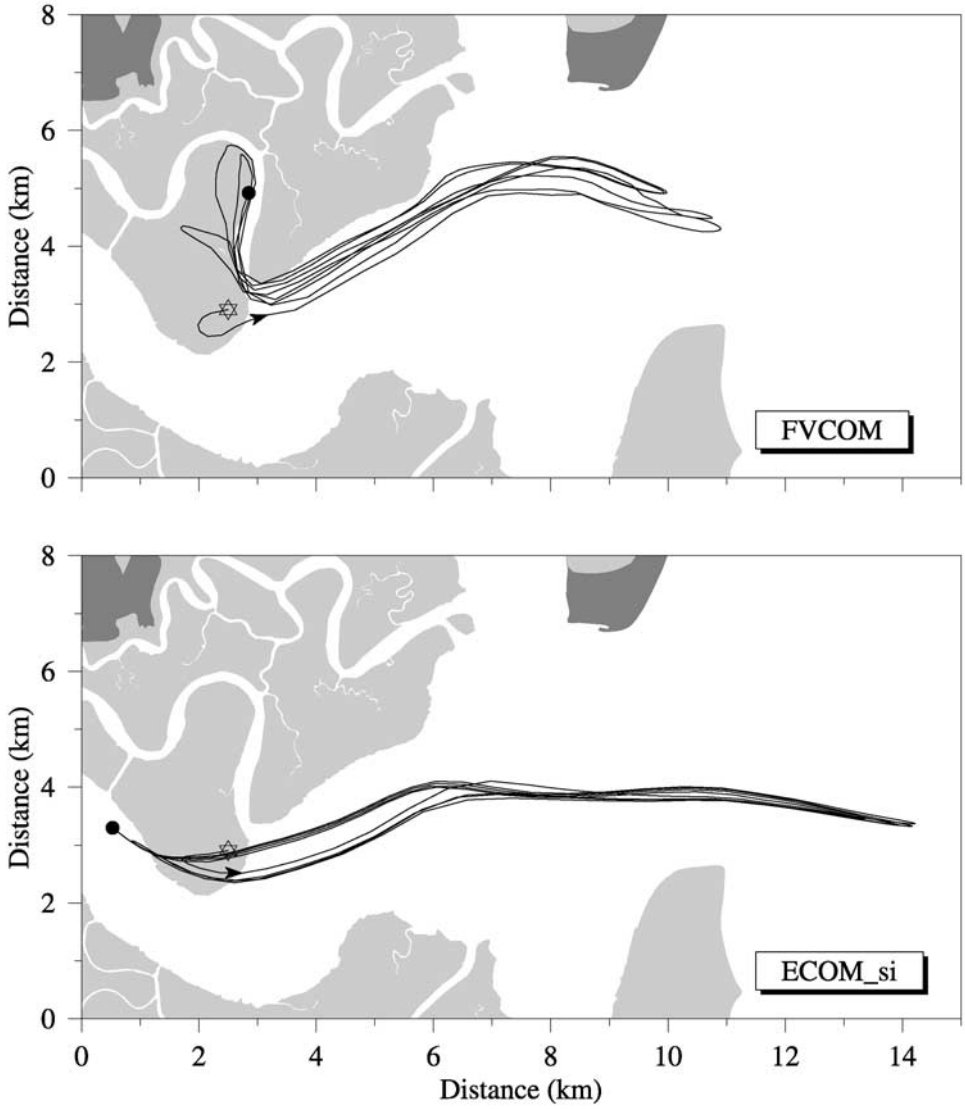

Figure 15. Comparison of a particle trajectory predicted by FVCOM and ECOM-si models. In this case, the particle was released at mean high water. Star, the release site; filled circle, the end location.

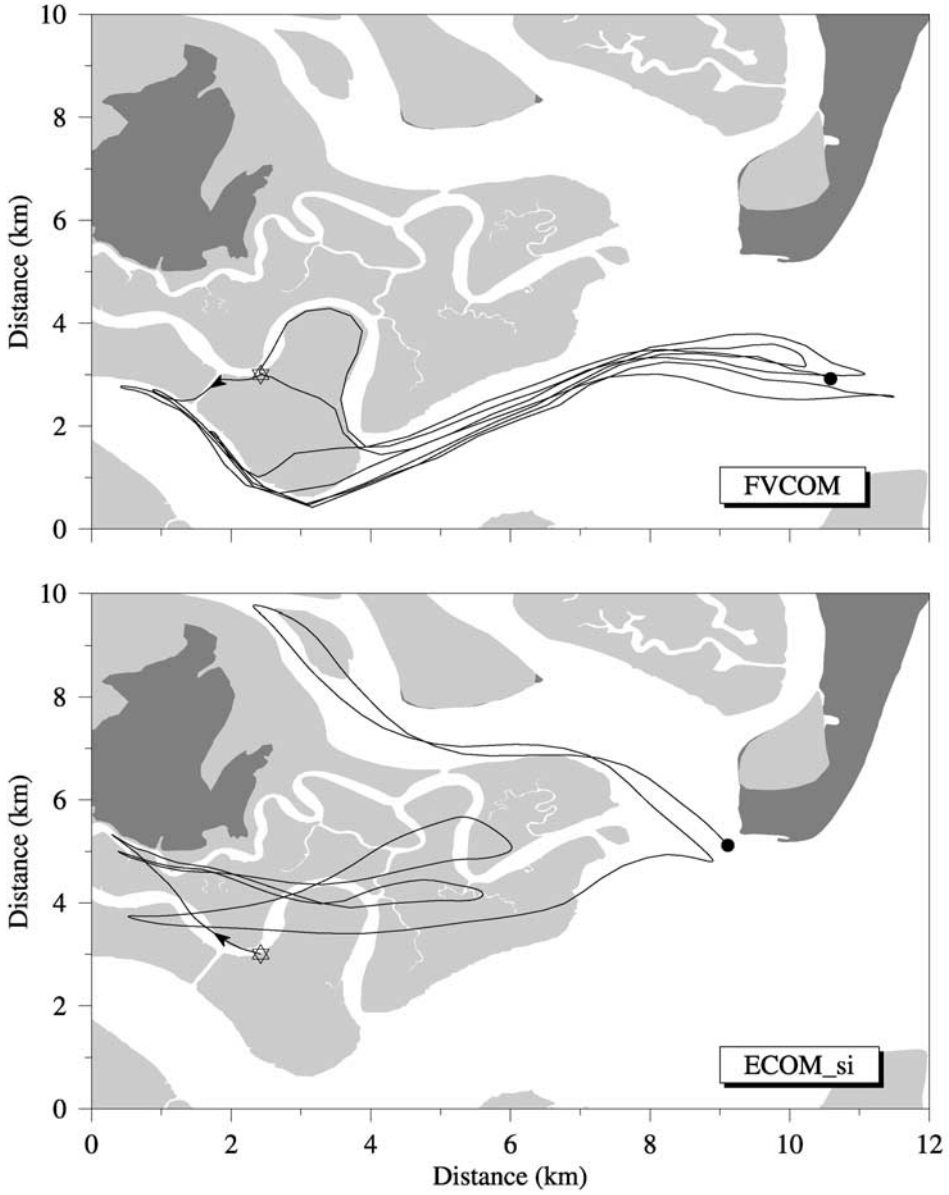

Figure 16. Comparison of a particle trajectory predicted by FVCOM and ECOM-si models. In this case, the particle was released at mean low water. Star, the release site; filled circle, the end location.

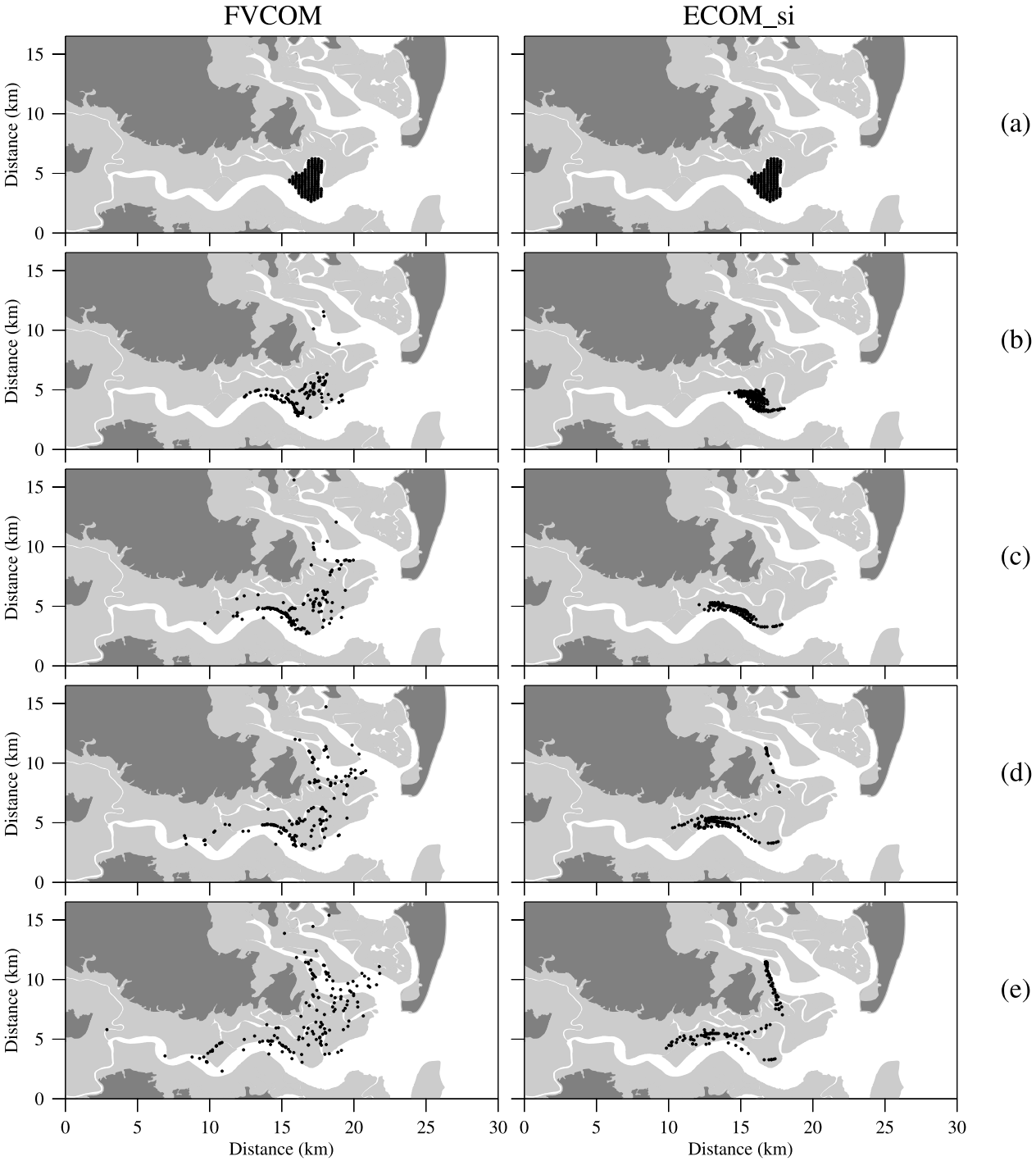

Figure 17. Comparison of particle trajectories predicted by (left) FVCOM and (right) ECOM-si models. In this case, a group of particles were released with uniform vertical distribution over the salt marsh at mean high water. Figures 17a–17f indicate the distributions of particles over each tidal cycle after release.

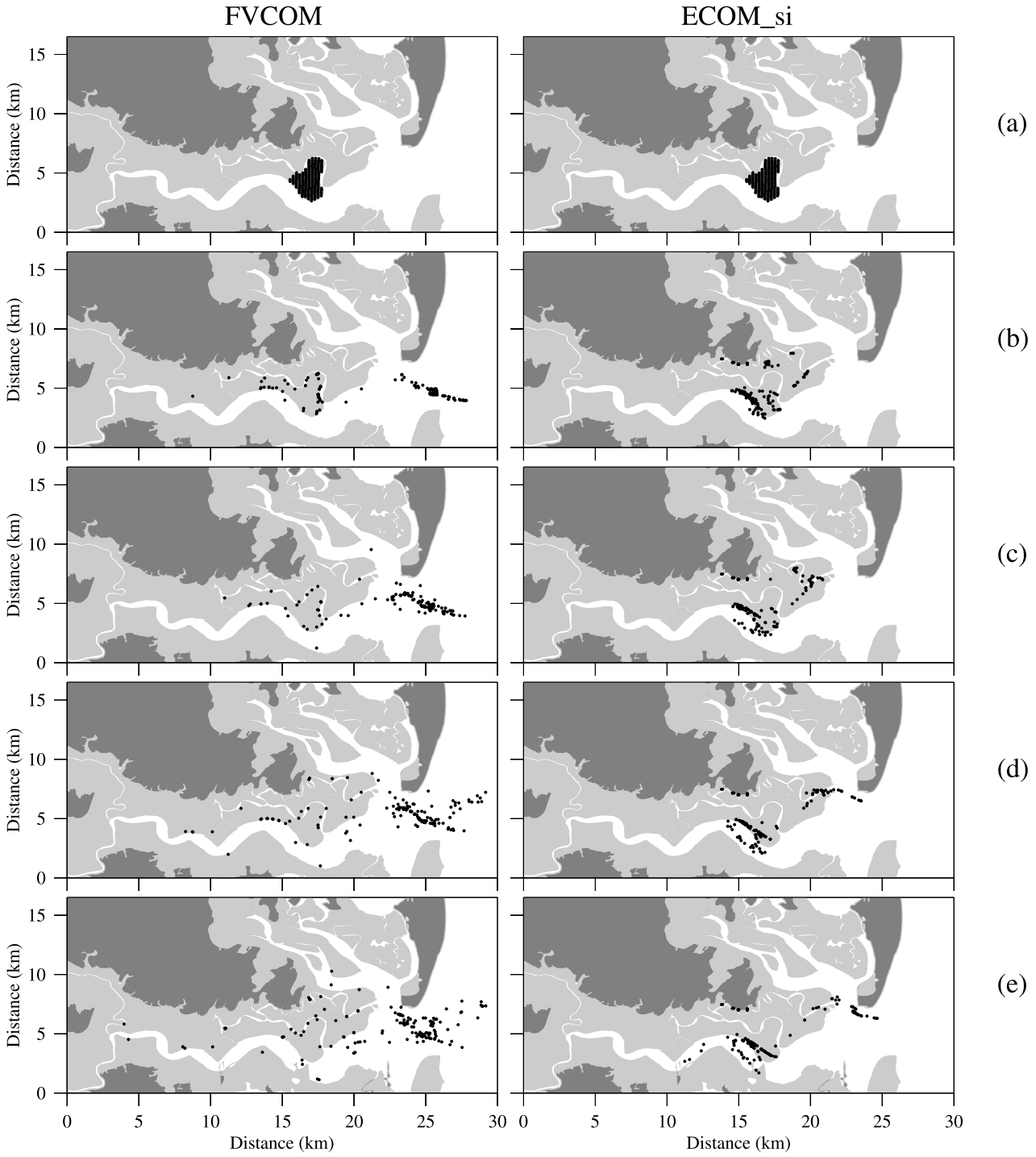

Figure 18. Comparison of particle trajectories predicted by (left) FVCOM and (right) ECOM-si models. In this case, a group of particles were released with uniform vertical distribution over the salt marsh at mean low water. Figures 18a–18f indicate the distributions of particles over each tidal cycle after release.

[41] **Acknowledgments.** This research was supported by the Georgia Sea grant (NA26RG0373 and NA66RG0282), the NOAA grant (NA16OP2323), and the NSF grants (OCE0234545, OCE0606928, OCE0712903, OCE0732084, and OCE0726851) for C. Chen, by the Georgia Sea grant (RR746-007/7512067, R/HAB-12-PD, R/HAB-18-PD, RR746-011/7876867), Georgia DNR (RR 100-279-9262764), and NSF grant (OCE-0554674) for C. Li. We thank Jack Blanton at SKIO for providing the CTD, water elevation, and current data used for the model validation. These data were used in our previous ECOM-si experiments and adopted again for FVCOM experiments. The observations were collected through support to SKIO provided by the Georgia Coastal Zone Management Program (grant RR100-279/9262764), the National Science Foundation (LMER grant DEB-9412089), LTER grant OCE-9982133), and a grant from the Georgia General Assembly. We thank Harvey Seim for sharing his preliminary analysis of the ADCP survey data with us when we were at the University of Georgia. Finally, we thank Mac Rawson for his encouragement and help in project organization. Hedong Liu, a former research associate at SMAST/UMASSD, used to be a member of the Satilla River Estuary FVCOM development team. His contributions are acknowledged here.

References

Alber, M., and J. E. Sheldon (1999), Use of a data-specific method to examine variability in the flushing times of Georgia estuaries, *Estuarine Coastal Shelf Sci.*, *49*, 469–482.

Blanton, J. O., C. Alexander, M. Alber, and G. Kineke (1999), The mobilization and deposition of mud deposits in a coastal plain estuary, *Limnologica*, *29*, 293–300.

Blumberg, A. F. (1994), A primer of ECOM3D-si, technical report, 66 pp., HydroQual, Inc. Mahwah, N. J.

Burchard, H. (2002), *Applied Turbulence Modeling in Marine Waters*, 215 pp., Springer, Berlin.

Chen, C., H. Liu, and R. Beardsley (2003), An unstructured grid, finite-volume, three-dimensional, primitive equations ocean model: Application to coastal ocean and estuaries, *J. Atmos. Oceanic Technol.*, *20*(1), 159–186.

Chen, C., G. Cowles, and R. C. Beardsley (2004), An unstructured grid, finite-volume coastal ocean model: FVCOM user manual, 1st ed., *SMAST/UMASSD Tech. Rep. 04-0601*, 183 pp., School for Marine Science and Technology, University of Massachusetts-Dartmouth, New Bedford, MA.

Chen, C., Z. Wu, R. C. Beardsley, S. Shu, and C. Xu (2005), Using MM5 to hindcast the ocean surface forcing fields over the Gulf of Maine and Georges Bank region, *J. Atmos. Oceanic Technol.*, *22*(2), 131–145.

Chen, C., G. Cowles, and R. C. Beardsley (2006a), An unstructured grid, finite-volume coastal ocean model: FVCOM user manual, 2nd ed., *SMAST/UMASSD Tech. Rep. 06-0602*, 315 pp., School for Marine Science and Technology, University of Massachusetts-Dartmouth, New Bedford, MA.

Chen, C., R. C. Beardsley, and G. Cowles (2006b), An unstructured grid, finite-volume coastal ocean model (FVCOM) system: Special Issue entitled "Advances in Computational Oceanography", *Oceanography*, *19*(1), 78–89.

Chen, C., H. Huang, R. C. Beardsley, H. Liu, Q. Xu, and G. Cowles (2007), A finite-volume numerical approach for coastal ocean circulation studies: Comparisons with finite-difference models, *J. Geophys. Res.*, *112*, C03018, doi:10.1029/2006JC003485.

Cowles, G. W. (2008), Parallelization of the FVCOM Coastal Ocean Model, *Int. J. High Performance Comput. Appl.*, in press.

Dudhia, J., D. Gill, K. Manning, W. Wang, C. Bruyere, J. Wilson, and S. Kelly (2003), PSU/NCAR mesoscale modeling system tutorial class notes and user's guide, MM5 modeling system version 3, Mesoscale and Microscale Meteorol. Div., Natl. Cent. for Atmos. Res., 390 pp.

Huang, H., C. Chen, G. Cowles, C. D. Winant, R. C. Beardsley, K. S. Hedstrom, and D. B. Haidvogel (2008), FVCOM Validation Experiments: Comparisons with ROMS for Three Idealized Test Problems, *J. Geophys. Res.*, doi:10.1029/2007JC004557, in press.

Kobayashi, M. H., J. M. C. Pereira, and J. C. F. Pereira (1999), A conservative finite-volume second-order-accurate projection method on hybrid unstructured grids, *J. Comput. Phys.*, *150*, 40–45.

Li, C., C. Chen, D. Guadagnoli, and I. Y. Georgiou (2008), Geometry induced residual eddies in estuaries with curved channel-observations and modeling studies, *J. Geophys. Res.*, *113*, C01005, doi:10.1029/2006JC004031.

Mellor, G. L., and T. Yamada (1982), Development of a turbulence closure model for geophysical fluid problem, *Rev. Geophys. Space Phys.*, *20*, 851–875.

Pieterzak, J., J. B. Jakobson, H. Burchard, H. J. Vested, and O. Petersen (2002), A three-dimensional hydrostatic model for coastal and ocean modeling using a generalized topography following co-ordinate system, *Ocean Modell.*, *4*, 173–205.

Seim, H., J. Blanton, and S. Elston (2006), Tidal circulation and energy dissipation in a shallow, sinuous estuary, *Ocean Dyn.*, *56*, 360–375, doi:10.1007/s10236-006-0078-x.

Smagorinsky, J. (1963), General circulation experiments with the primitive equations. part I: The basic experiment, *Mon. Weather Rev.*, *91*, 99–164.

Zheng, L., C. Chen, and H. Liu (2003a), A modeling study of the Satilla River Estuary, Georgia. part I: Flooding/drying process and water exchange over the salt marsh-estuary-shelf complex, *Estuaries*, *26*(3), 651–669.

Zheng, L., C. Chen, M. Abler, and H. Liu (2003b), A 3-D modeling study of the Satilla River estuarine System. part II: Suspended sedimentation, *Estuaries*, *26*(3), 670–679.

R. C. Beardsley, Department of Physical Oceanography, Woods Hole Oceanographic Institution, Woods Hole, MA 02543, USA.

C. Chen and J. Qi, School for Marine Science and Technology, University of Massachusetts-Dartmouth, 868 South Rodney French Boulevard, New Bedford, MA 02744, USA. (c1chen@umassd.edu)

K. Gates, H. Lin, and R. Walker, Marine Extension Service, University of Georgia, Athens, GA 30602, USA.

C. Li, Coastal Studies Institute, Department of Oceanography and Coastal Sciences, School of the Coast and Environment, Louisiana State University, Baton Rouge, LA 70803, USA.